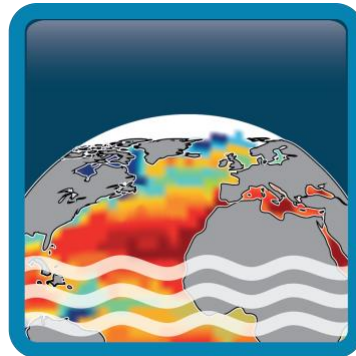# Climate Change Initiative+ (CCI+) Phase 2

Sea Surface Salinity

Algorithm Development Plan (ADP)
Customer: ESA
Ref.: ESA-CCI-PRGM-EOPS-SW-17-0032

Version: v5.0
Revision Date: 07/11/2024
Filename: SSS_cci-D2.4-ADP_v5.0.docx
Deliverable code: D2.4

Signatures

Author	Nicolas Reul (Science Leader)		27/11/2024
Reviewed by	Rafael Catany		
Approved by	Jacqueline Boutin (Science Leader)		30/10/2024
	Nicolas Reul (Science Leader)		30/10/2024
	Rafael Catany (Project Manager)		30/10/2024
	Roberto Sabia (Technical Officer)		
Accepted by	Susanne Mecklenburg (Technical Officer) ESA		

Diffusion List
Sea Surface Salinity Team Members
ESA (Susanne Mecklenburg, Roberto Sabia, Paolo Cipollini)

Amendment Record Sheet

Date / Issue	Description	Section / Page
07/11/2022 / v4.0	Circulation ADP first CRDP for CCI Salinity phase 2 (April 2023 to April 2026)	New document
30/10/2024/ v5.0	ADP second CRDP for CCI Salinity phase 2	

Table of Contents

List of figures

List of tables

No table of figures entries found.

1 Introduction

1.1 Scope of this document

This document holds the Algorithm Development Plan (ADP) prepared by CCI+ team, as part of the activities included in the [WP210] of the Proposal (Task 2 from SoW ref. ESA-CCI-PRGM-EOPS-SW-17-0032).

This document summarizes the planned algorithm developments to be performed for the CCI+SSS project phase-2 activity.

1.2 Structure of the document

This document is composed of 3 sections and present the plan for the development of the CCI-SSS algorithm that are proposed for the 1st CRDP, along to the evolution plan for the second CRDP. **Section 1** is an introduction presenting the scope, reference and applicable documents, acronyms, and the structure of the document. **Section 2** present the plan for the algorithms of L-band sensor-based SSS algorithms and which form the core of the CCI-SSS products. In **Section 3**, we detail the algorithm development for CCI-SSS algorithms based on C and X-band data and in **section 4**, we provide summary and next steps.

1.3 References

1.3.1 Applicable Documents

ID	Document	Reference
AD01	CCI+ Statement of Work	SoW
AD02	Product User Guide (PUG)	PUG
AD03	User Requirement Document (URD)	SSS_cci-D1.1-URD-i1r0
AD04	Product Specification Document (PSD)	SSS_cci-D1.2-PSD-v1r4
AD05	Algorithm Theoretical Baseline Document	SSS_cci-D2.3-ATBD_L3_L4-i1r0_v1.1
AD06	Algorithm Development Plan (ADP) for CCI-SSS 1st phase	SSS_cci-D2.4-ADP_v3.1

1.3.2 Reference Documents

ID	Document	Reference
RD01	Boutin, J., N. Martin, N. Kolodziejczyk, and G. Reverdin (2016a), Interannual anomalies of SMOS sea surface salinity, *Remote Sensing of Environment*	doi:http://dx.doi.org/10.1016/j.rse.2016.02.053

ID	Document	Reference
RD02	Kolodziejczyk, N., J. Boutin, J.-L. Vergely, S. Marchand, N. Martin, and G. Reverdin (2016), Mitigation of systematic errors in SMOS sea surface salinity, *Remote Sensing of Environment*	doi:http://dx.doi.org/10.1016/j.rse.2016.02.061.
RD03	Liang Hong, Normal Kuring, Joel Gales and Fred Patt (2017), AQ-014-PS-0017_Aquarius_L2toL3ATBD_DatasetVersion5.0	
RD04	Fred Patt, Liang Hong (2017), AQ-014-PS-0018_AquariusLevel2specification_DatasetVersion5.0	
RD05	Meissner, T. and F. J. Wentz, 2016: Remote Sensing Systems SMAP Ocean Surface Salinities [Level 2C, Level 3 Running 8-day, Level 3 Monthly], Version 2.0 validated release. Remote Sensing Systems, Santa Rosa, CA, USA.	www.remss.com/missions/smap, doi:10.5067/SMP20-2SOCS
RD06	Boutin J., J.-L. Vergely, S. Marchand, F. D'Amico, A. Hasson, N. Kolodziejczyk, N. Reul, G. Reverdin, J. Vialard (2018), New SMOS Sea Surface Salinity with reduced systematic errors and improved variability, *Remote Sensing Of Environment*	doi:http://dx.doi.org/10.1016/j.rse.2018.05.022
RD07	Yiwen Zhou ; Roger H. Lang ; Emmanuel P. Dinnat ; David M. Le Vine (2017), L-Band Model Function of the Dielectric Constant of Seawater, *IEEE Transactions on Geoscience and Remote Sensing* (Volume: 55 , Issue: 12)	
RD08	Gaillard F. (2015), ISAS-13 temperature and salinity gridded fields. SEANOE.	http://doi.org/10.17882/45945.
RD09	Reul Nicolas, Saux Picart Stephane, Chapron Bertrand, Vandemark D., Tournadre Jean, Salisbury J. (2009). Demonstration of ocean surface salinity microwave measurements from space using AMSR-E data over the Amazon plume. Geophysical Research Letters (GRL) , 36, 1-5 .	https://doi.org/10.1029/2009GL038860
RD10	Qingtao Song and Zhaohui Wang. (2017). Sea surface salinity observed from the HY-2A satellite. Satellite Oceanography and Meteorology, vol.2 (1): 41–48.	http://dx.doi.org/10.18063/SOM.2017.01.004.
RD11	Wentz, F. J., and T. Meissner (2000), AMSR ocean algorithm, version 2, algorithm theoretical basis document, RSS Tech. Rep. 121599A-1, Remote Sens. Syst., Santa Rosa, Calif.	
RD12	Wentz, F. J. and T. Meissner, (2007), AMSR-E Ocean Algorithms; Supplement 1, report number 051707, 6 pp., Remote Sensing Systems, Santa Rosa, CA.	
RD13	Meissner, T., and F. J. Wentz, (2012), The emissivity of the ocean surface between 6 - 90 GHz over a large range of wind speeds and Earth incidence angles, IEEE TGRS, 50(8), 3004-3026.	
RD14	Webster, W. J., T. T. Wilheit, D. B. Ross, and P. Gloersen (1976), Spectral characteristics of the microwave emission from a wind-driven foam-covered sea, J. Geophys. Res., 18, 3095–3099.	
RD15	Dinnat, E.P.; Le Vine, D.M.; Boutin, J.; Meissner, T.; Lagerloef, G. Remote Sensing of Sea Surface Salinity: Comparison of Satellite and In Situ Observations and Impact of Retrieval Parameters. *Remote Sens.* **2019**, *11*, 750.	

Climate Change Initiative+ (CCI+)
Phase 2
Algorithm Development Plan

Ref.: ESA-CCI-PRGM-EOPS-SW-17-0032
Date: 07/11/2024
Version: v5.0
Page: 3 of 38

ID	Document	Reference
RD16	Olivier, L., G. Reverdin, A. Hasson, and J. Boutin (2020), Tropical Instability Waves in the Atlantic Ocean: Investigating the Relative Role of Sea Surface Salinity and Temperature From 2010 to 2018, Journal of Geophysical Research: Oceans, 125(12), e2020JC016641, doi:https://doi.org/10.1029/2020JC016641	
RD17	Akhil, V. P., J. Vialard, M. Lengaigne, M. G. Keerthi, J. Boutin, J. L. Vergely, and F. Papa (2020), Bay of Bengal Sea surface salinity variability using a decade of improved SMOS re-processing, Remote Sensing of Environment, 248, 111964, doi:https://doi.org/10.1016/j.rse.2020.111964.	
RD18	Reverdin, G., et al. (2021), Formation and Evolution of a Freshwater Plume in the Northwestern Tropical Atlantic in February 2020, Journal of Geophysical Research: Oceans, 126(4), e2020JC016981, doi:10.1029/2020jc016981.	
RD19	Kerr, Y., et al. (2019), Low Frequency Passive Microwave User Requirement Consolidation Study, Issue 2, *Rep. SO-TN-CB-GS-0075*, CESBIO, Toulouse, https://mycore.core-cloud.net/index.php/s/Y3tpySnNhl9HWUH	
RD20	Fournier, S., and T. Lee (2021), Seasonal and Interannual Variability of Sea Surface Salinity Near Major River Mouths of the World Ocean Inferred from Gridded Satellite and In-Situ Salinity Products, Remote Sensing, 13(4), 728.	
RD21	Yu, L., F. M. Bingham, T. Lee, E. P. Dinnat, S. Fournier, O. Melnichenko, W. Tang, and S. H. Yueh (2021), Revisiting the Global Patterns of Seasonal Cycle in Sea Surface Salinity, Journal of Geophysical Research: Oceans, 126(4), e2020JC016789, doi:https://doi.org/10.1029/2020JC016789.	
RD22	Bingham, F. M., S. Brodnitz, and L. Yu (2021), Sea Surface Salinity Seasonal Variability in the Tropics from Satellites, Gridded In Situ Products and Mooring Observations, Remote Sensing, 13(1), 110.	
RD23	Melnichenko, O., P. Hacker, N. Maximenko, G. Lagerloef, and J. Potemra (2016), Optimum interpolation analysis of Aquarius sea surface salinity, Journal of Geophysical Research: Oceans, 121(1), 602-616, doi:https://doi.org/10.1002/2015JC011343.	
RD24	Nardelli, B., R. Droghei, and R. Santoleri (2016), Multi-dimensional interpolation of SMOS sea surface salinity with surface temperature and in situ salinity data, Remote Sensing of Environment, 180, 392-402, doi:https://doi.org/10.1016/j.rse.2015.12.052.	
RD25	Kolodziejczyk, N., M. Hamon, J. Boutin, J.-L. Vergely, G. Reverdin, A. Supply, and N. Reul (2021), Objective Analysis of SMOS and SMAP Sea Surface Salinity to Reduce Large-Scale and Time-Dependent Biases from Low to High Latitudes, Journal of Atmospheric and Oceanic Technology, 38(3), 405-421, doi:10.1175/jtech-d-20-0093.1.	
RD26	Boutin, J., J.-L. Vergely, E. P. Dinnat, P. Waldteufel, F. D'Amico, N. Reul, A. Supply, and C. Thouvenin-Masson (2021), Correcting Sea Surface Temperature Spurious Effects in Salinity Retrieved From Spaceborne L-Band Radiometer Measurements, IEEE Transactions on Geoscience and Remote Sensing, 59(9), 7256-7269, doi:10.1109/tgrs.2020.3030488.	
RD27	Kao, H.-Y., G. S. E. Lagerloef, T. Lee, O. Melnichenko, T. Meissner, and P. Hacker (2018), Assessment of Aquarius Sea Surface Salinity, Remote Sens., 10(9):1341.	
RD28	Fournier, S., T. Lee, X. Wang, T. W. K. Armitage, O. Wang, I. Fukumori, and R. Kwok (2020), Sea Surface Salinity as a Proxy for Arctic Ocean Freshwater Changes, Journal of Geophysical Research: Oceans, 125(7), e2020JC016110, doi:https://doi.org/10.1029/2020JC016110.	

ID	Document	Reference
RD29	Brucker, L., E. P. Dinnat, and L. S. Koenig (2014), Weekly gridded Aquarius L-band radiometer/scatterometer observations and salinity retrievals over the polar regions – Part 2: Initial product analysis, The Cryosphere, 8(3), 915-930, doi:10.5194/tc-8-915-2014.	
RD30	Olmedo, E., C. Gabarró, V. González-Gambau, J. Martínez, J. Ballabrera-Poy, A. Turiel, M. Portabella, S. Fournier, and T. Lee (2018), Seven Years of SMOS Sea Surface Salinity at High Latitudes: Variability in Arctic and Sub-Arctic Regions, Remote Sensing, 10(11), 1772	
RD31	Supply, A., J. Boutin, J.-L. Vergely, N. Kolodziejczyk, G. Reverdin, N. Reul, and A. Tarasenko (2020b), New insights into SMOS sea surface salinity retrievals in the Arctic Ocean, Remote Sensing of Environment, 249, 112027, doi:https://doi.org/10.1016/j.rse.2020.112027.	
RD32	Tang, W., S. Yueh, D. Yang, A. Fore, A. Hayashi, T. Lee, S. Fournier, and B. Holt (2018), The Potential and Challenges of Using Soil Moisture Active Passive (SMAP) Sea Surface Salinity to Monitor Arctic Ocean Freshwater Changes, Remote Sensing, 10(6), 869.	
RD33	Vazquez-Cuervo, J., C. Gentemann, W. Tang, D. Carroll, H. Zhang, D. Menemenlis, J. Gomez-Valdes, M. Bouali, and M. Steele (2021), Using Saildrones to Validate Arctic Sea-Surface Salinity from the SMAP Satellite and from Ocean Models, Remote Sensing, 13(5), 831.	
RD34	Tarasenko, A., A. Supply, N. Kusse-Tiuz, V. Ivanov, M. Makhotin, J. Tournadre, B. Chapron, J. Boutin, N. Kolodziejczyk, and G. Reverdin (2021), Properties of surface water masses in the Laptev and the East Siberian seas in summer 2018 from in situ and satellite data, Ocean Sci., 17(1), 221-247, doi:10.5194/os-17-221-2021.	
RD35	Supply, A., J. Boutin, J.-L. Vergely, N. Martin, A. Hasson, G. Reverdin, C. Mallet, and N. Viltard (2018), Precipitation Estimates from SMOS Sea-Surface Salinity, Quarterly Journal of the Royal Meteorological Society, 144(S1), 103-119, doi:https://doi.org/10.1002/qj.3110.	
RD36	Supply, A., J. Boutin, G. Reverdin, J.-L. Vergely, and H. Bellenger (2020a), Variability of Satellite Sea Surface Salinity Under Rainfall, in Satellite Precipitation Measurement: Volume 2, edited by V. Levizzani, C. Kidd, D. B. Kirschbaum, C. D. Kummerow, K. Nakamura and F. J. Turk, pp. 1155-1176, Springer International Publishing, Cham, doi:10.1007/978-3-030-35798-6_34.	
RD37	Hasson, A., M. Puy, J. Boutin, E. Guilyardi, and R. Morrow (2018), Northward Pathway Across the Tropical North Pacific Ocean Revealed by Surface Salinity: How do El Niño Anomalies Reach Hawaii?, Journal of Geophysical Research: Oceans, 123(4), 2697-2715, doi:https://doi.org/10.1002/2017JC013423.	
RD38	Boutin, J., N. Martin, G. Reverdin, S. Morisset, X. Yin, L. Centurioni, and N. Reul (2014), Sea surface salinity under rain cells: SMOS satellite and in situ drifters observations, Journal of Geophysical Research: Oceans, 119(8), 5533-5545, doi:https://doi.org/10.1002/2014JC010070	

1.4 Acronyms

AD	Applicable Document
ATBD	Algorithm Theoretical Basis Document
Aquarius	NASA mission

CCI	The ESA Climate Change Initiative (CCI) is formally known as the Global Monitoring for Essential Climate Variables (GMECV) element of the European Earth Watch programme
CCI+	Climate Change Initiative Extension (CCI+), is an extension of the CCI over the period 2017–2024
CMEMS	Copernicus Marine Environmental Monitoring Service
DARD	Data Access Requirements Document
DOI	Digital Object Identifier
DPM	Detailed Processing Model
ECMWF	European Centre for Medium Range Weather Forecasts
ECV	Essential Climate Variable
EO	Earth Observation
FOV	Field Of View
Hs	Significant Wave Height (see also SWH)
KS	Klein and Swift sea water dielectric constant model
MW	Meissner and Wentz sea water dielectric constant model
NASA	National Aeronautics and Space Administration
NOAA	National Oceanic and Atmospheric Administration
NOP	Numerical Ocean Prediction
NWP	Numerical Weather Prediction
OTT	Ocean Target Transform
SSS	Sea Surface Salinity
SST	Sea Surface Temperature
SWH	Significant Wave Height (see also Hs)
TBC	To Be Completed
UCR/CECR	Uncertainty Characterisation Report (formerly known as the Comprehensive Error Characterisation Report)
URD	User Requirements Document
VOS	Volunteer Observing ships
WS	Wind Speed

2 Plan for L-band data based CCI+SSS Algorithms

2.1 Input Level 2/Level 3 Data

For the 1st CRDP of CCI+SSS phase 2, the input data to the CCI algorithms are levels 2 for SMOS and SMAP or Level 3 for Aquarius sensor. These data are all projected on the CCI+SSS Level 4 grid (a regular 0.25° grid (instead of over a EASE2 25km grid during phase 1) for the global product, the EASE 2 polar grids for the polar products). They are the following for each sensor:

- **SMOS:** for the global products, we will use as input L2 products generated by the SMOS ESA L2 v700 chain. These products are provided onto an ISEA grid at 15km resolution. SSS is classified according to the distance to the sub-satellite track and into ascending and descending passes. For polar products, we will also test the use of polar CCI level 2 SSS produced during phase 1 (v671 obtained from ERA5 auxiliary data over polar grids). Several retrieved SSS will be tested (SSS retrieved with or without wind speed retrieval, as tested in v671 retrievals).
- **SMAP:** as in CCI+SSS phase 1, we will use the RSS Level 2 v5.0 products. These are swath SSS from SMAP provided daily at 40 km resolution. The data are split into ascending and descending products and between the fore and aft views.
- **Aquarius:** as in CCI+SSS phase 1, we will use as input the official release products L3 v5.0, which is the official end of mission public data release from the AQUARIUS/SAC-D mission. Daily Aquarius Level 3 sea surface salinity (SSS) at 1-degree spatial resolution are used.

2.2 Grid change

During CCI+SSS phase 1, L3 and L4 products were generated on the EASE equatorial grid. During CCI+SSS phase 2, L3 products will be delivered on a 0.25° regular grid. L4 products will be delivered on a 0.25° regular grid and on two polar EASE grids, one for high northern latitudes, one for high southern latitudes.

The projection algorithms on the 3 above mentioned grids depend on the input product:

- SMOS and SMAP data are reprojected using a nearest neighbour criteria.

- For Aquarius data set, the current phase 1 interpolation will be kept. It is a weighting of the 4 nearest neighbours according to the inverse of the square of the distance.

2.3 Level 2 preconditioning

Pre-processing algorithms will be developed in particular to correct some seasonal latitudinal biases and to mitigate some intermittent RFI biases.

2.3.1 Seasonal biases correction.

During phase 1, significant seasonal biases appeared at intermediate and high latitudes. These biases affect all sensors. They have been partially corrected on SMOS and not at all on Aquarius and SMAP.

On SMOS, they have been corrected by self-referencing (latitudinal seasonal correction). We propose to correct them by taking ISAS as reference. The same will be done for SMAP and Aquarius.

For the new polar products, several approaches will be investigated. At very high latitudes, ISAS is not well suited to serve as a reference (ISAS is very poorly constrained due to the lack of in situ measurements). It is a matter of self-referencing by identifying the sensor(s) that are the least affected by seasonal biases mainly related to the presence of the ice vicinity. These biases are particularly important because of the very low SST encountered in these regions. These seasonal biases cannot be properly corrected latitudinally. Therefore, a grid node by grid node seasonal correction approach is considered. Two different ways will be tested for the calculation of this correction depending on how the SMOS-SMAP-Aquarius data are collocated. Indeed, it is possible to compare the data on a monthly or weekly average basis. Weekly averages would better account for the intra-monthly variability of the ice edge position.

2.3.2 RFI mitigation.

The RFIs mainly affect SMOS and to a much less extent SMAP and Aquarius. We propose to implement an algorithm that allows correcting the temporal variations of RFI biases based on a regional principal component analysis (PCA). This correction is estimated according to the across-swath position, to the orbit orientation and the region considered. It is then applied on the SMOS levels 2 and gives rise to L2 intermediate products. These intermediate products are the input of the L3 and L4 algorithms.

For the first CRDP, this correction will be applied on two or three regions only.

This correction is not applied on Aquarius nor on SMAP.

2.4 Plan for L3 algorithms

L3 products will be derived using the same methodology as in CCI+SSS phase 1.

They are, by definition, time and space-averaged products obtained sensor by sensor, without mixing inter-sensor information. Here, we consider simple averages of swath Level 2 SSS products, which may have been already corrected for some biases (e.g. land sea contamination or spatio-temporal drifts corrections in the brightness temperatures of the instrument such as the Ocean Target Transformation). These products can thus be used as a reference in terms of observed SSS variability since we don't apply to the observed SSS any specific smoothing operation (for example, by allowing introducing representativity errors or variance filtering).

A priori, these products will not be distributed to users except upon specific requests. They will be made available as part of the validation and verification of products and will serve to build up the Level 4 products.

They will be delivered on a 0.25° regular grid (same grid as L4 products).

The space-time aggregation of the input data will be calculated for each grid node and on a daily or decade temporal sliding window. Using an average weighted by the errors σ_i^2 of each SSS product.

The monthly L3 products contain the averaged SSS field and the associated error for each L-band sensor: SMOS, Aquarius and SMAP.

2.5 Plan for L4 algorithms

2.5.1 Data coverage

During CCI+SSS phase 1, the data coverage was found to be insufficient, especially at high latitudes. The filtering algorithms will be modified to increase the data coverage.

2.5.2 Global L4 product algorithm

The algorithm for merging the various products will be mostly in line with the one used during phase 1.

This algorithm is a Bayesian optimal interpolation that takes into account:

-the uncertainties of the input L2 products

-the a priori variability on the SSS fields

-the representativeness errors

The Phase 1 algorithm simultaneously estimates the inter-sensor biases and the SSS time series grid node by grid node. The biases are considered constant over time.

We propose to implement a change in the algorithm in order to be able to take into account biases that vary in time. To do so, we will consider predefined periods on which the bias is constant but can differ from one period to another. The algorithm ensures the continuity of the SSS between periods. Once implemented, we will decide whether or not to use it for the generation of L4 products.

2.5.3 L4 polar algorithm

After correcting for seasonal bias (see Section 2.3.1) at Level 2, an OI identical to that of Phase 1 will be conducted. Several strategies will be tested:

-different seasonal corrections

-use of the estimated SSS with or without wind speed retrieval

-with or without seasonal correction

-with or without absolute bias correction

2.5.4   L4 products content and coverage

In the first CRDP, the global product will cover the period 01/2010-10/2022. The research polar product will either cover the period 01/2010-11/2020 if based on the SMOS v671 L2 product or the same period as the global product if the latter is of at least as good quality as v671 derived polar product.

As in CCI phase 1, the following fields will be included in the L4 products:

-monthly and weekly SSS fields: obtained from OI algo

-SSS uncertainty: obtained from OI algo

-number of outliers over the considered time interval (+/-30 days for monthly data and +/-10 days for weekly data).

-number of data over the considered time interval (+/-30 days for monthly data and +/-10 days for weekly data).

-SSS quality flag

-ice flag

-pct_var : 100x(SSS error)²/variability (%)

These values will be given for each grid node and sampled every two weeks for monthly products and every day for weekly products.

2.6   Plan for the evolution of the L-band CCI algorithms for 2nd CRDP

For the CRDP 2, we plan to adjust some components of the radiative transfer model used in the SMOS SSS retrieval and to rerun the L2OS processor using SMOS L1 v7, ERA5 auxiliary parameters and ISAS to derive SMOS OTT, in order to get a more stable SMOS SSS time series. Adjustments of L2OS processor will be based on:

- new L2OS model components studied in the frame of the ESLs (Tb-wind and dielectric constant models),

-possible evolution of Tb-wind model to consider possible systematic differences between ERA5 and ECMWF forecasts auxiliary parameters

-possible evolution of Tb-wind model to adjust SMOS, SMAP and Aquarius models based on colocations of Tb (we do not foresee to reprocess SMAP and AQUARIUS SSS but a SSS correction based on the DSSStheo approach (as described in the CCI phase 2 proposal) might be envisaged).

Other evolutions of the L2 and L4 algorithms will be studied to answer as much as possible feedbacks from the climate users about the first CRDP of CCI+SSS phase 2.

It is worth noting that the planned work is primarily aimed at algorithmic improvements based on the satellite data already acquired. In case the SMOS or SMAP instrument would stop working, the activities would be little impacted, and the time series would continue to be produced but with a lower quality during the period with only one instrument. If both instruments ceased to operate, the time series would be discontinued, but the planned work would continue to be relevant.

2.7 Plan for the evolution to CCI L4 version 5 for 2nd CRDP

Version 5 products will cover the period: Jan 2010- Dec 2023,

During the first semester of 2024, L2 SSS that will be ingested in CCI L4 version 5 are prepared as follows :

- A CCI SMOS L2 reprocessing has taken place with:
  ◦ ERA5 (wind, SST, atm. variables) priors (instead of ECMWF forecasts)
  ◦ Use of ISAS SSS for OTT computation
  ◦ Several configurations (with/without WS retrieval, Acard, correction or mitigation for wave flags issues)
  ◦ Better coverage close to the coast
- SMAP SSS v5.3 (instead of SMAP v5.0) will be used
- Aquarius v3 : no change
-

For the Level 4 reprocessing: flags are to be redefined, and a specific RFI processing (Bonjean et al. 2024) is extended to most parts of the global ocean.

As of July 2024, the status of the L4 v5 reprocessing is as follows :

- SMOS L2OS configuration set-up in February (RFI filtering and various inversion confs) *done*.
- L2OS upgrade: end of February (correction of sea state flags, and of sunglint) *done*
- Hybrid algorithm for RFI processing: end of March, code done ; end of June,application to new SMOS L2 *done*.
- Preparation of SMAP v5.3 data: February. *Done*
- AUX_ECMWF and ISAS product download update: February *done*

- OTT calculation & validation (including commissioning period): February-March *done*
- L2OS start-up: 1 year of processing & UDP verification : February *done*
- Start of processing for entire period & verification : March *done*
- Commissioning period processing: end of March *done*
- Preparation of SMOS data for L4 processing: mid-April (RFI post processing, SST, WS correction, lat, WS, flags definition ...) *done*
- L4 processing: a L4 processing v5.1 (same steps as processing v4.41 but with different input L2 described above, and including an updated RFI mitigation applied to most ocean regions) July 2024 *done,* verifications (LOCEAN) ongoing
- PVASR preparation: July to August (provisional)

Provisional agenda for validation team and climate users:

L4 product validation: August to late October

CAR: early November 2024, end April 2025

L2 and L3 generation: to be determined according to requirements

3   Plan for C- and X-band data based CCI SSS algorithm

3.1   Introduction and Summary of phase-1 achievements

Before 2010, in situ measurements were the only source of SSS estimates. Argo profiler data is the main source of basins-scale SSS salinity data, and Argo data was extremely sparse in the major tropical river plume regions, such as the Amazon-Orinoco, Mississippi, Congo/Niger or the Bay of Bengal river plume regions, particularly before 2002. The accumulation of Argo and previous hydrological data over time now allows depicting the seasonal variations of SSS in these region very well. On the other hand, the Argo network coverage was insufficient to produce basin-scale seasonal SSS maps, and hence unable to describe SSS interannual variations before the advent of SSS remote sensing. Satellite SSS observation only started with ESA's SMOS (2010-now), followed by NASA's Aquarius (2011-2015) and SMAP (2015-now) missions. These three satellites are all equipped with microwave radiometers operated at L-band (central frequency ~1.4 GHz) a frequency for which the response of the sea surface emissivity to SSS is highest. While the SMOS SSS retrievals were initially highly contaminated by radio-frequency interferences and other sources of land contamination, improved bias corrections later allowed strongly improved SMOS SSS retrievals with roughly similar performances to Aquarius and SMAP, with correlations and rms-differences to co-located in situ data of 0.8, and 0.6 pss, respectively in average in the four above mentioned regions. Data from the SMOS, Aquarius, and SMAP radiometers then allowed to describe interannual SSS signals. Yet, the SSS satellite record (12 years) is too short to confidently describe interannual SSS signals, or SSS variability on longer time scales, such as the long-term freshening expected in these regions due to the expected hydrological cycle intensification in response to anthropogenic forcing. This is mainly because of sparse in situ observations prior the full deployment of the Argo float network and the relatively recent L-band satellite radiometer era.

The Advanced Microwave Scanning Radiometer - Earth Observing System (AMSR-E) onboard Aqua satellite has microwave channels spanning the 6.9 - 89.0 GHz range (including the 6.9 (C-band) to 10.7 GHz (X-band) frequencies). AMSR-E was initially designed for monitoring atmospheric water, SST, and surface winds over the ocean. However, the C- and X-band channels also display some sensitivity to SSS at high SST, although much weaker than at L-band (at the AMSR-E incidence angle of 55° and at an SST ~30°C, the perfectly flat sea surface brightness temperature sensitivity to SSS in vertical polarization: $\partial Tb / \partial SSS$ ~-0.05 K/pss, and, less than -0.01 K/pss , for C- and X- band, respectively, against ~0.9 K/pss at L-Band (Reul et al., 2009).Reul et al., (2009) noted that C- and X- bands have a roughly similar sensitivity to SST and surface roughness, and that the C- minus X-band emissivity contrast keeps sensitive to SSS (~0.05 K/pss) and is much less affected by SST and surface roughness. They used that approach to estimate SSS in the Amazon River plume region. This is made possible by the high SST (which maximize the sensitivity to SSS) and strong salinity contrasts (because the low sensitivity results in a poor accuracy). Such principle has recently been applied to retrieve SSS from HY2-A data for the freshwater runoff near the Yangtze Delta. The Congo-Niger, Mississippi, and BoB also displays

high SST (with most of the basin above 20 °C all year long) and very strong salinity contrasts. In this project, we investigate if the concept of Reul et al. (2009) can be applied to AMSR-E C/X bands data to reconstruct SSS over the 2002-11 period, hence yielding an almost 20-year-long satellite SSS record. Note that HY-2A was launched in 2011. Note also that WindSat's radiometer performed C- and X-band brightness temperature measurements since 2003 [23] but which are not publicly available. Hence, the datasets from both sensors are not considered for the 1st CRDP of CCI-SSS project.

The algorithm is mainly based on the Radiative Transfer Model (RTM) of Meissner and Wentz (hereafter MW12) and was described in detail in [AD 06]. Necessary empirical adjustments to the RTM and the empirical inversion model linking the C- minus X-band emissivity to SSS were first developed in phase-1. Those were specifically determined for each of the river plume region's conditions using co-located brightness temperatures (T_B), surface wind, water vapor, cloud liquid water, and SST data from AMSR-E, as well as SSS data from SMOS and Aquarius/SAC-D, all collected during the common operation period of these satellites (June 2010-September 2011). These algorithms were then used to produce monthly-averaged SSS fields for each region, at a spatial resolution of ~60 km and gridded at ¼°x¼° from May 2002 to Sep 2011.

During CCI-SSS project phase-1,

❑ we developed first algorithms to retrieve monthly 0.25°x0.25° SSS from AMSR-E data for four specific river plume dominated warm oceanic regions (AORP, MRP, CNRP, and BoB)
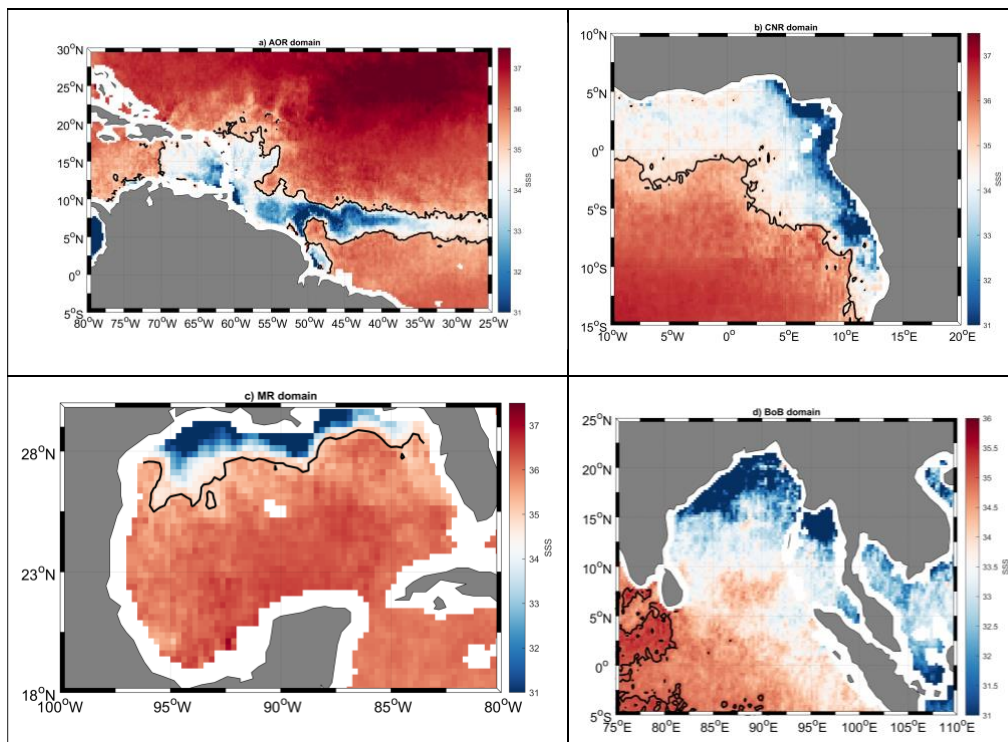
❑ Several algorithms options were investigated (additional empirical refinements wrt Wentz & Meissner 2012's ATBD) and several types of SSS inversion algorithm (empirical GMF, Neural Network) were tested

❑ Both ascending and descending passes surface emissivity frequency differential contrasts were merged as input to the algorithm,

❑ The auxiliary SST products used in the phase-1 algorithms is the CCI SST ESA Sea Surface Temperature Climate Change Initiative (SST_cci): Level 4 Analysis Climate Data Record, version 2.1.

❑ The 21 monthly maps of CCI L-band SSS v3.21 data from January 2010 to September 2011, common with AMSR-E, have been used to train the algorithms

❑ We finally selected a two layer feed-forward neural network (NN) with 40 Neurones per layers for each region. We used a Bayesian Regularized Artificial Neural Networks to regularize the Network towards reducing bias and variance. (A high-variance state is a state when the network is overfitted). So far, we have tested NN with 2 hidden layers and 40 Neurones per layers using as input data the surface emissivity frequency differential contrasts after atmospheric corrections and the extra polynomial empirical adjustments (wind, sst, clw, wv). Retrieval tests will be conducted in phase-2 with, or without these extra polynomial empirical adjustments to determine in which conditions do the NN inversion performs better. As found, one of the remaining issue is the relatively low number of training observations for the freshest SSS which lead, in parts, to overestimation of SSS from AMSR-E in the freshest SSS zones. To better characterize these conditions, the distance to coast has been further used as an input to the NN. Verification over the common period exhibit a 0.3-0.6 pss RSMSD between the training CCI SSS and the retrieved AMSR-E SSS.

❑ The data of the full AMSR-E operation period (Oct 2002-Sep 2011) have been processed at Ifremer to generate monthly first 'research' products.

❑ These first products were validated against in situ data from the CORA database over 2002-2009. Note that we found that the CORA datasets in these regions are still including some spurious SSS observations (in particular TSG data) we were not filtered out for a rough assessment of the AMSR-E SSS. First analyses revealed that the root Mean Square Difference (RMSD) between AMSR-E based and in situ SSS is found to be about twice the RMSD between L-band CCI v3.2 SSS and in situ in the four regions. As found, one of the major remaining issue is the systematic overestimation of the freshest SSS by the NN inversion, whatever the region.

3.2 Plan for the evolution of the C/X-band CCI algorithms for 1st CRDP

At the beginning of phase 2, we found significant differences in the spatio-temporal variability of the estimated sea surface brightness temperature frequency differential contrasts ΔTb between ascending and descending passes for all four river plume regions. These differences are particularly evident along the coastlines within a band of about ~150 kms from the nearest coastlines. This is illustrated for the Amazon and Orinoco River plume region in Figure 1 showing the differences in the temporal Median Absolute Deviation in between ascending and descending passes:
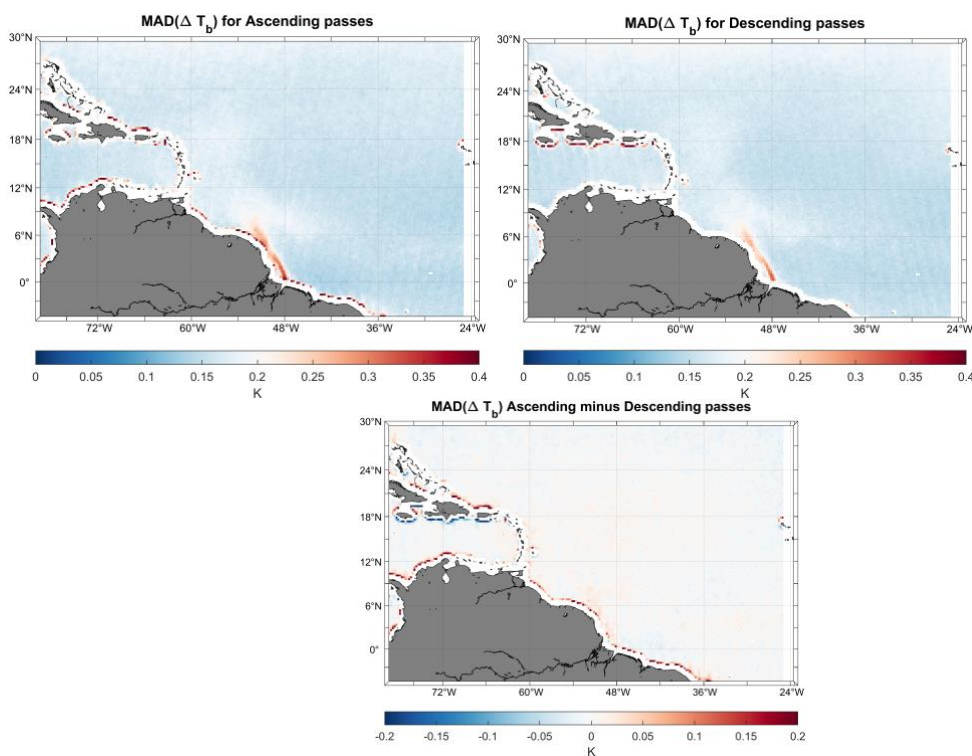

Figure 1: Temporal MAD over may 2002 to October 2011 of the surface brightness temperature frequency differential contrasts ΔTb for ascending : (Top left) and descending passes : (Top right). Bottom difference between ascending and descending passes MAD.

As found, the temporal MAD over May 2002 to October 2011 of the surface brightness temperature frequency differential contrasts ΔTb is showing a similar signal associated with the Amazon River plume in both ascending and descending passes. However, a different signal variability is observed within a band following the coastlines with higher variability found north and south of the coastlines for ascending, and descending passes, respectively, as illustrated in Figure 1, bottom plot. Very similar type of behaviours were found for the 3 other remaining regions (not shown here). This evidences a potential remaining land contamination in the AMSR-E Tb data. As these potentially contaminated data were not filtered out in phase-1 for developing the NN retrievals and as high ΔTb contrasts are associated with low SSS, this issue could explain part of the systematic overestimation of the freshest SSS by the NN inversion.

The plan for the algorithm development of the first CDRP of phase-2 therefore includes a first step:

Step 1) filtering out/masking the input ΔTb where the MAD strongly differ between ascending and descending passes before training the NN.

In addition, looking back at AMSR-E SST products, we also realized that the diurnal cycles in SST might be particularly important in the studied regions (see examples for the BoB in Figure 2).
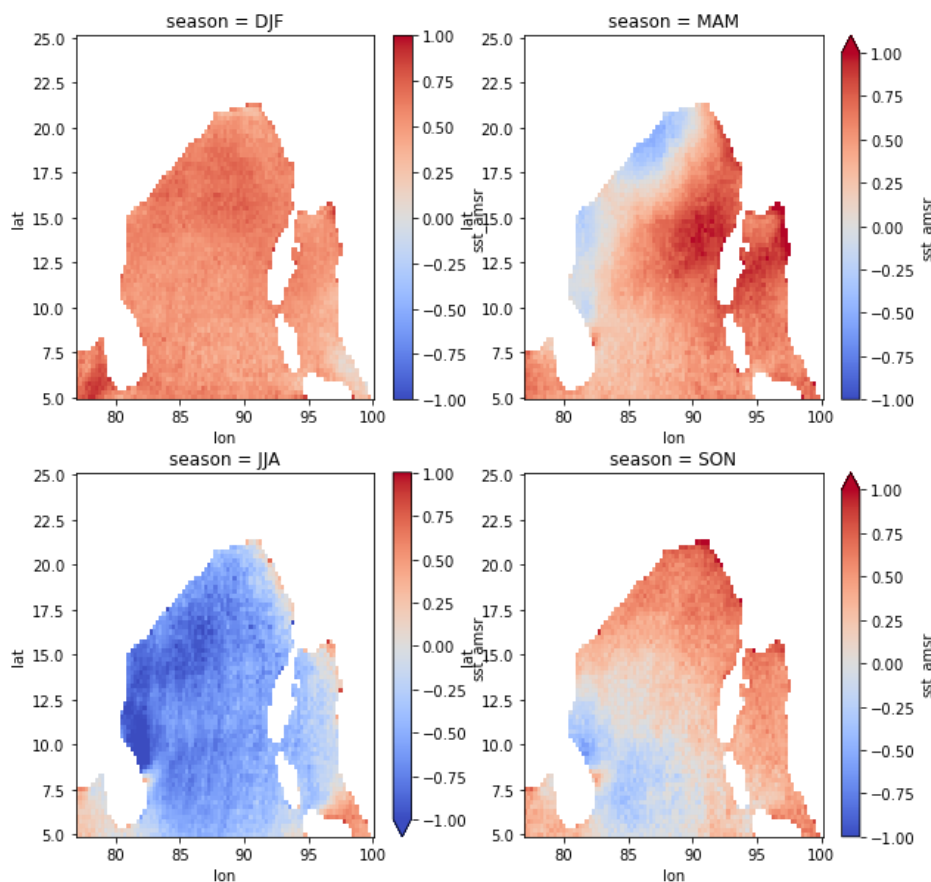

Figure 2: Mean differences between AMSR-E L2B SST retrieved in ascending (1:30 pm local time) and descending passes (1:30 am local time) for the four seasons and the BoB.

As the auxiliary SST products used as input to our NN algorithm, in phase-1, we used the CCI SST ESA Sea Surface Temperature Climate Change Initiative (SST_cci): Level 4 Analysis Climate Data Record, version 2.1. This product is based on IR data only and is adjusted to a 25 cm depth and corresponds to a nighttime 'mean' SST. Given that 1) the penetration depth at C- and X-band is ~1 cm and 2) that the ascending passes are measurements conducted at a local time of 1:30 pm, strong biases can be expected using the CCI L4 SST IR daily data as an input to our algorithm. The reason why we choose such product is a) to develop cross-ECV activities and 2) this SST analysis is independent from AMSR-E SST data themselves. Note that an SSS monthly climatology (World Ocean Atlas, [28]) is used to correct for the average SSS impact on the AMSR-E brightness

temperature used in the SST retrieval. In phase-2, first CDR, given the above consideration, we now plan a second step:

Step 2) use AMSR-E SST as input to the NN SSS inversion algorithms, instead of CCI SST and assess the impact on retrieved SSS quality.

As both Land Sea contamination and diurnal cycles (SST, wind, water vapour, etc..) affect ascending and descending passes differently, it might be better for each region to develop NN inversion algorithms separately for ascending and descending passes than by combining the data from both type of passes. We plan the following development step:

Step 3) NN Retrieval tests will be conducted for ascending and descending passes separately or by merging both passes to determine in which conditions do the NN inversion performs better.

In phase-1, we developed an ensemble of empirical (polynomial) adjustments to the MW's12 RTM model including wind, sst, cloud liquid water, and water vapour corrections. We determined these functions from a residual analyses of the ΔTbs using the 21 month common period between CCI L band SSS and AMSR-E data.

Step 4) Retrieval tests will be conducted with, and, without, these extra polynomial empirical adjustments to determine in which conditions do the NN inversion performs better than our empirical fitting functions based on residual data analyses.

Finally, in phase-1, we validated the output of the first NN inversion algorithms using CORA datasets which are including some spurious SSS observations (in particular TSG data). To characterize the error in our first CDRP C/X-band SSS products we shall:

Step 5) use the EN4 validated data to best estimate the NN L3 SSS errors and to define quality levels (e.g. as a function of distance to coast, wind regimes, etc ...)

As found, one of the remaining issue is the systematic overestimation of the freshest SSS. This bias was found systematically in all four regions and using either an empirical bivariate inversion algorithm SSS=f(ΔTb, SST), or, the NN inversion methods. It is likely, that part of these biases are associated with the spatial sampling of AMSR-E with respect to in situ local sampling. A detail analysis of the spatio-temporal representatitivity errors of AMSR-E SST is therefore needed. We will therefore conduct:

Step 6) Analyses of the representativity error will be conducted for the specific spatial (~60 km) and temporal resolution (monthly) of AMSR-E SSS using high resolution (1/36°) model outputs in the four regions.

Climate Change Initiative+ (CCI+)
Phase 2
Algorithm Development Plan

Ref.: ESA-CCI-PRGM-EOPS-SW-17-0032
Date: 07/11/2024
Version: v5.0
Page: 18 of 38

3.3   Algorithm plan for C-/X-band L3 SSS of the 2nd CRDP of phase-2

For the 2nd CRDP of phase-2, we plan five major steps:

- Step 1: Develop algorithms (NN) for WindSat Tbs data developed for the four above regions for the training periods
- Step 2: Validate against CCI and in situ data over 4 years of data and adjust step 1 if needed
- Step 3: generation of the WindSat SSS dataset back to 2003
- Step 4: merge AMSR-E and WindSat SSS products
- Step 5: extension to other potential regional River plume regions including Yangtze and Mekong river plumes.

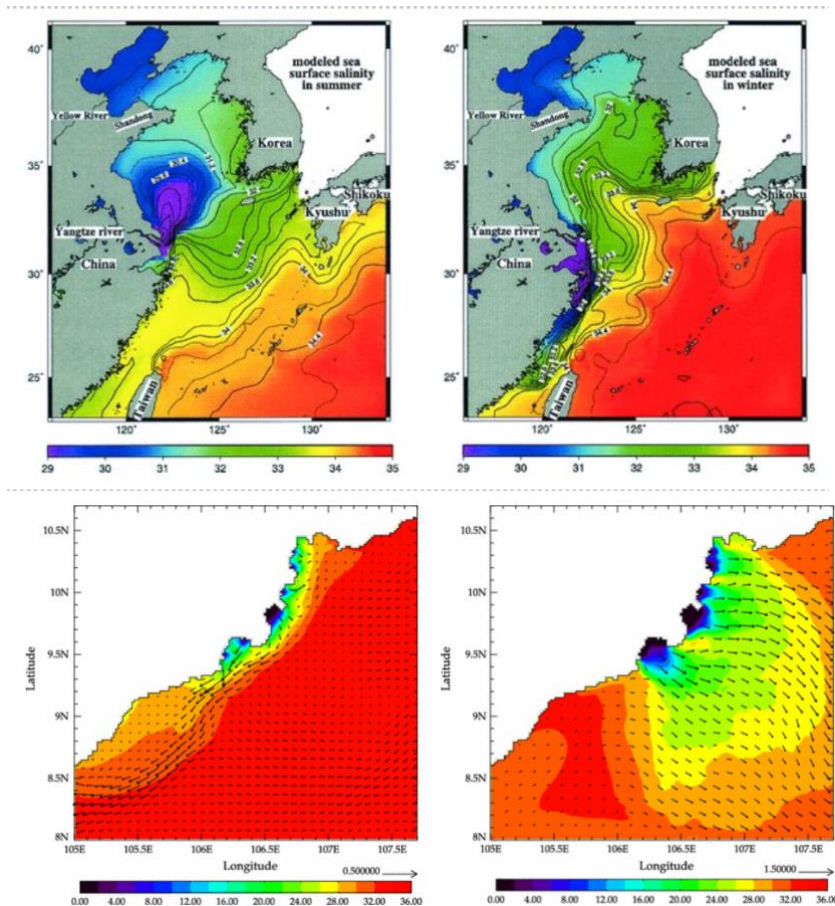*Figure 3: Top :Yangtze river plume region. Bottom: Mekong River Plume*

These are very challenging regions because of potential coastal contaminations, RFI contaminations (both in C- and L-band) and the Yangtze river plume region can exhibit cold waters in winter (< 10°C). However, these regions show very large seasonal SSS gradients and could be potentially well monitored with AMSR-E and WindSAt.

We are now developing SSS retrieval algorithm based on WindSat data as described below.

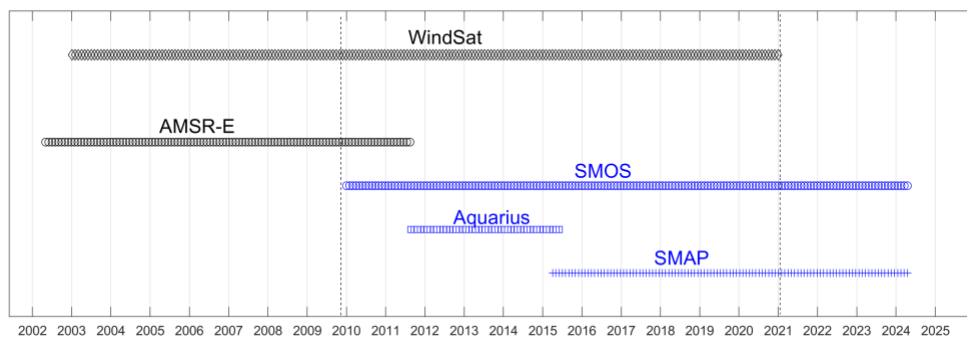## 3.4 Algorithm plan for WindSat C-/X-band L3 SSS of the 2nd CRDP

Figure 4: timetable of the operation periods of AMSR-E, WindSAt, SMOS, SMAP and Aquarius.

The complete archive of WindSat Tbs are now available at REMSS with 10 years of common operation period with L-band sensors including SMOS, Aquarius and SMAP and with improved NEDT at C- (0.48K) and X-band (0.37K) with respect to AMSR-E data (> 0.6 K). The WindSat Polarimetric Radiometer was developed by the Naval Research Laboratory (NRL) Remote Sensing Division and the Naval Center for Space Technology for the U.S. Navy and the National Polar-orbiting Operational Environmental Satellite System (NPOESS) Integrated Program Office (IPO). It was launched on January 6, 2003 aboard the Department of Defense Coriolis satellite. WindSat was meant to demonstrate the capabilities of a fully polarimetric radiometer to measure the ocean surface wind vector from space. Prior to launch, the only instrument capable of measuring ocean wind vectors were scatterometers (active microwave sensors). In addition to wind speed and direction, the instrument can also measure sea surface temperature, soil moisture, ice and snow characteristics, water vapor, cloud liquid water, and rain rate.

Here we plan to develop an SSS inversion algorithm to WindSat Tbs following a similar approach than the one used for AMSR-E. The Neural Network SSS inversion algorithm shall clearly be improved in terms of robustness thanks to the very long training period. Details on the ADP are provided here below.

3.4.1 WindSat Instrument Description

Table 1 summarizes the WindSat channels and their properties while Figure 5 shows the WindSat antenna footprints projected on the surface of the earth.

Table 1: . Overview of WindSat channels. Polarization basis: 1=vertical (V), 2=horizontal (H), 3= +45 (P), 4= -45 (M), 5=left circular (L), 6=right circular (R). BW = band width. τ = integration time,

NEDT = noise equivalent delta T, EIA = earth incidence angle, IFOV – individual field of view footprint.

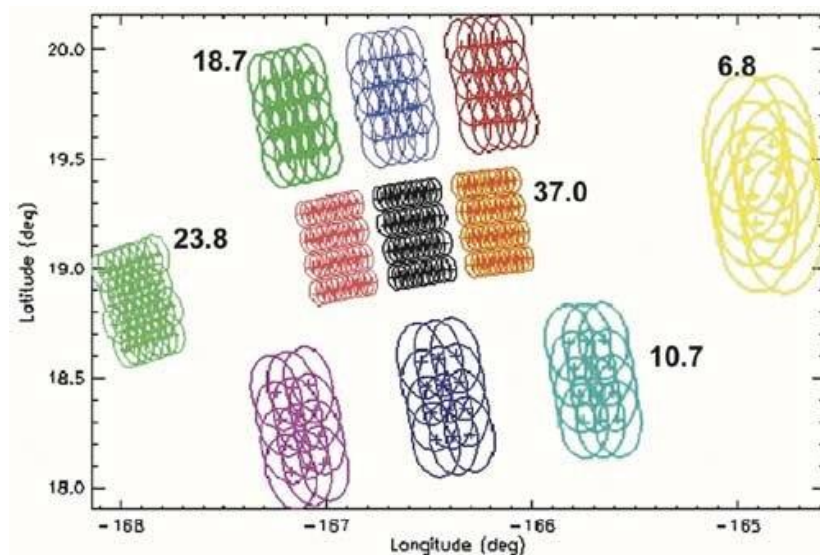| Frequency [GHz]	Polarizations	BW [MHz]	τ [msec]	NEDT	EIA [deg]	IFOV [km x km]
6.8	VH	125	5.00	0.48	53.8	39 x 71
10.7	VH PM LR	300	3.50	0.37	50.1	25 x 38
18.7	VH PM LR	750	2.00	0.39	55.6	16 x 27
23.8	VH	500	1.48	0.55	53.2	20 x 30
37.0	VH PM LR	2000	1.00	0.45	53.2	8 x 13

Figure 5: WindSat antenna footprints projected on the surface of the earth. The figure shows a subset of four scans. Note that all frequencies are Nyquist sampled in the along-scan direction. One can see the relative sampling rate among the frequency bands.

3.4.2   WindSat Tb and Geophysical products

WINDSAT data will be added into the approach developed for AMSR-E with two objectives being enhanced data coverage and solidification of the CX-band SSS inversion approach. This includes looking at potentially systematic errors in the requisite atmospheric corrections that impact surface brightness temperature estimates.   Data across 2010-2021 will be first used to evaluate empirically-observed windspeed, SST and salinity dependence in both X-band and C-band data and to develop a CCI-SSS v4.41 informed algorithm.   Combined AMSRE/WINDSAT mapping of SSS for the four river plume regions will then be prepared. The input data are provided below:

3.4.2.1   RSS WindSat Calibrated Top of the Atmosphere Level 1C Brightness Temperatures Version 8.0

This dataset contains the Level 1C WindSat Top of the Atmosphere (TOA) TB processed by Remote Sensing Systems RSS (https://www.remss.com/missions/windsat/). The WindSat radiances are turned into TOA TB after correction for hot and cold calibration anomalies [5], receiver non-linearities [3,5], sensor pointing errors [1,5], antenna cross-polarization contamination [2,5], spillover [2,5], Faraday rotation [1,5] and polarization alignment [1,5]. The data are resampled on a fixed regular 0.125 deg Earth grid using Backus-Gilbert Optimum Interpolation. The sampling is done separately for fore and aft looks. The 10.7, 18.7, 23.8, 37.0 GHz channels are resampled to the 10.7 GHz spatial resolution (35 km). The 6.8 GHz channels are given at their native spatial resolution (50 km). The 10.7, 18.7, 23.8, 37.0 GHz channels are absolutely calibrated using the GMI sensor as calibration reference [5,6]. The 6.8 GHz channels are calibrated using the open ocean with the RSS ocean emission model [4,7] and the Amazon rain forest [3] as calibration targets.   The data are gridded at a resolution of the fixed Earth which is 1/8 =0.125 deg. Filter (QA/QC): Swath L2A Ta and L2B EDRs based on standard product flags.

3.4.2.2   RSS WindSat Environmental Data Records (EDR)

The current version of Remote Sensing Systems WindSat geophysical data products is v7.0.1 and they provide a suite of environmental data in one file for each day. The data suite contains the measurements listed in Table 2.

Table 2: *WindSat ocean measurements in the order provided in RSS binary data files. Effective spatial resolution for each measurement varies from the 0.25 deg grid the data are mapped to. Channel polarizations are listed as V for Vertical, H for Horizontal, P for +45 deg, L for Left Circular, and R for Right Circular.*

Ocean Measurement	Acronym	Effective Spatial Resolution [km x km]	Channels for Retrieval	Required
Time	TIME	N/A	N/A	

Sea surface temperature	SST	39 x 71	6.8 VH, 10.7 VH,18.7 VH, 23.8 VH, 37.0 VH
Ten-meter wind speed using low frequency channels	WSPD_LF	25 x 38	10.7 VH, 18.7 VH, 23.8 VH, 37.0 VH
Ten-meter wind speed using medium frequency channels	WSPD_MF	16 x 27	18.7 VH, 23.8 VH, 37.0 VH
Columnar atmospheric water vapor	VAPOR	16 x 27	18.7 VH, 23.8 VH, 37.0 VH
Columnar cloud liquid water content	CLOUD	16 x 27	18.7 VH, 23.8 VH, 37.0 VH
Rain rate	RAIN	8 x 13	18.7 VH, 23.8 VH, 37.0 VH
All-weather 10-meter wind speed	WSPD_AW	25 x 38 no rain 39 x 71 in rain	6.8 VH, 10.7 VH, 18.7 VH, 23.8 VH, 37.0 VH
Ten-meter wind direction (relative to north)	WDIR	25 x 38	10.7 VHPMLR, 18.7 VHPMLR, 23.8 VH, 37.0 VHPMLR

WindSat data products include the standard set of measurements (sea surface temperature, wind speed, water vapor, cloud liquid water, and rain rate) and include additional measurements with respect to AMSR-E:

- WDIR: Because of its polarimetric channels, WindSat can measure surface wind direction. WDIR is only provided if the wind speed exceeds 3 m/s and the rain rate is below 15 mm/hr. The wind directions in the product are in oceanographic convention.

- WSPD_AW: If the 6.8 GHz channels are available together with all the other vertically and horizontally polarized channels, we can retrieve WindSat surface wind speed in both rain-free and rainy atmospheres. We combine various algorithms, including a global wind speed through rain algorithm that works under all rain conditions and an H-wind algorithm that has been specifically trained for tropical cyclones. The final all-weather wind speed, WSPD_AW, provided in the binary files is a smooth blend between the standard wind speed obtained in non-raining conditions WSPD_LF, the global wind speed through rain and the H-wind derived wind speed.

In addition to the all-weather wind speeds, RSS produce two standard rain-free radiometer wind products: WSPD_LF (low-frequency) and WSPD_MF (medium frequency). The first, WSPD_LF is created using the frequency channels at 10.7 GHz and above (see Table 2) and is most similar to the AMSR-E wind. The second, WSPD_MF, uses frequency channels at 18.7 GHz and above and is most similar to the SSM/I wind. Each wind product has distinct advantages. The WSPD_LF is less affected by the atmosphere and rain, but is affected by 10.7 GHz RFI and sun glitter effects. The WSPD_MF has a higher effective spatial resolution, is less affected by ice and land contamination, and only slightly affected by sun glitter effects, and RFI. The WSPD_MF are a little noisier than the WSPD_LF.

3.4.3   Plan for the WindSat Algorithm Development

We plan to split the common periods between WindSat and L-band sensors as follows:

- 7 years of data from 2012-2019 will be used to train the SSS inversion NN

- 4 years of data (2010-2012) and (2019-2021) will be used to validate the WindSat SSS retrievals
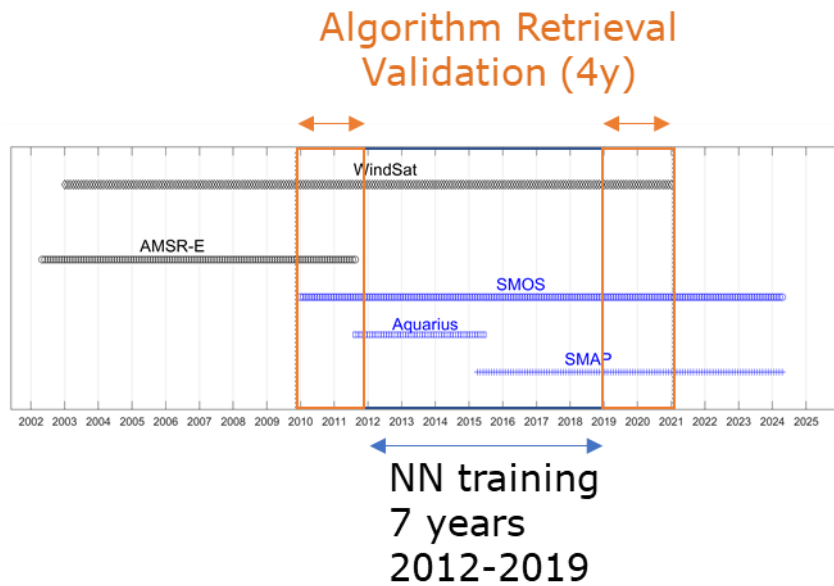
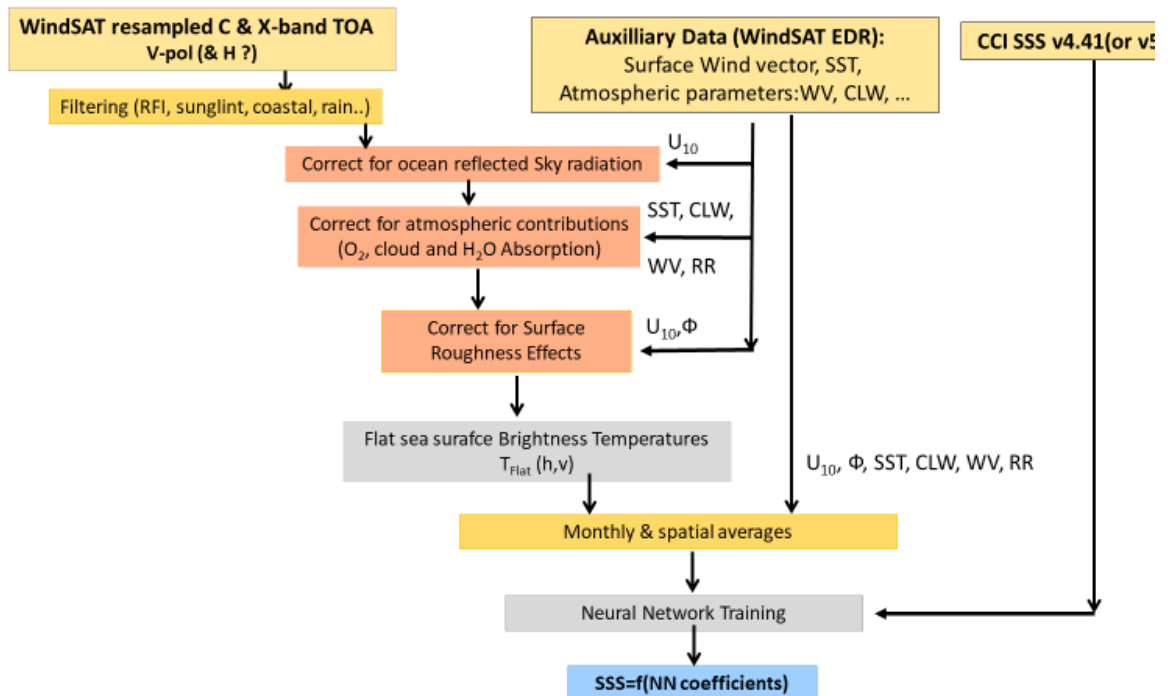*Figure 6: windSat SSS inversion NN training and Algorithm Validation periods*

Figure 7: Schematic of the WindSAt SSS inversion algorithm developements

As illustrated in Figure 7, using WidnSat Tbs, EDR and CCI-SSS v4.4 co-localized data over 2012-2019, the development of the WindSat SSS inversion algorithm will consist in:

- Derive the sea surface emissivity from Top of the Atmosphere Level 1C Brightness Temperatures based on the microwave radiation transfer model (RTM) of WM (2000,2012), and the flat and rough surface emissivity model (MW, 2012) with the EDR inputs. The aim is to derive a residual surface emissivity (presumably SSS and SST-dependent only) by applying the following corrections

  - Wind speed impact removal

  - 1st-order SST impact removal

  - The residual 2D Atmosphere impact removal

- Derive empirical NN coefficients of the SSS algorithms based on co-localized CCI-SSS for:

  - e_C: C-band emissivity and

    De: C- and X-band emissivity difference

The NN will then be applied to 4 years of data (2010-2012) and (2019-2021) to be validated against CCI SSS and in situ data.

4 Summary and way forward

4.1 CCI L-band global and polar phase 2 SSS plan

During CCI+SSS phase 1, L3 and L4 products were generated on the EASE equatorial grid. During CCI+SSS phase 2, L3 products will be delivered on a 0.25° regular grid.

Pre-processing algorithms will be developed for L2 data in particular to correct some seasonal latitudinal biases and to mitigate some intermittent RFI biases. During phase 1, significant seasonal biases appeared at intermediate and high latitudes. These biases affect all sensors. They have been partially corrected on SMOS and not at all on Aquarius and SMAP. A similar self-referencing method than the one used for SMOS using ISAS fields will be applied in phase-2 for SMAP and Aquarius. For the new polar products, several approaches will be investigated. The RFIs mainly affect SMOS and to a much less extent SMAP and Aquarius. We propose to implement an algorithm that allows correcting the temporal variations of RFI biases based on a regional principal component analysis (PCA). For the first CRDP, this correction will be applied on two or three regions only and for SMOS only.

L3 products will be derived using the same methodology as in CCI+SSS phase 1. A priori, these products will not be distributed to users except upon specific requests. They will be made available as part of the validation and verification of products and will serve to build up the Level 4 products.

During CCI+SSS phase 1, the L4 data coverage was found to be insufficient, especially at high latitudes. The filtering algorithms will be modified to increase the data coverage. The algorithm for merging the various products will be mostly in line with the one used during phase 1. We propose however to implement a change in the algorithm in order to be able to take into account biases that vary in time. To do so, we will consider predefined periods on which the bias is constant but can differ from one period to another. The algorithm ensures the continuity of the SSS between periods. Once implemented, we will decide whether or not to use it for the generation of L4 products. For the L4 polar products, after correcting for seasonal bias at Level 2, an OI identical to that of Phase 1 will be conducted. Several strategies will be tested including, different seasonal corrections, use of the estimated SSS with or without wind speed retrieval, with or without seasonal correction and with or without absolute bias correction. In the first CRDP, the global product will cover the period 01/2010-10/2022. The research polar product will either cover the period 01/2010-11/2020 if based on the SMOS v671 L2 product or the same period as the global product if the latter is of at least as good quality as v671 derived polar product.

For the CRDP 2, we plan to adjust some components of the radiative transfer model used in the SMOS SSS retrieval and to rerun the L2OS processor using SMOS L1 v7, ERA5 auxiliary parameters and ISAS to derive SMOS OTT, in order to get a more stable SMOS SSS time series.

Version 5 products will cover the period: Jan 2010- Dec 2023,

During the first semester of 2024, L2 SSS that will be ingested in CCI L4 version 5 are prepared as follows :

•   A CCI SMOS L2 reprocessing has taken place with:

◦   ERA5 (wind, SST, atm. variables) priors (instead of ECMWF forecasts)

◦   Use of ISAS SSS for OTT computation

◦   Several configurations (with/without WS retrieval, Acard, correction or mitigation for wave flags issues)

◦   Better coverage close to the coast

•   SMAP SSS v5.3 (instead of SMAP v5.0) will be used

•   Aquarius v3 : no change

For the Level 4 reprocessing: flags are to be redefined, and a specific RFI processing (Bonjean et al. 2024) is extended to most parts of the global ocean.

4.2   CCI C/X-band river plume phase 2 SSS plan

For the 2nd CRDP of phase-2, we plan five major steps:

- Step 1: Develop algorithms (NN) for WindSAt data developed for the four above regions for the training periods
- Step 2: Validate against CCI and in situ data over 2010-2012 and 2019-2021 and adjust step 1 if needed
- Step 3: generation of the WindSAt SSS dataset back to 2003
- Step 4: merge AMSR-E and WindSat SSS products
- Step 5: extension to other potential regional River plume regions including Yangtze and Mekong river plumes.

4.3   5.References

[1] T. Meissner and F. Wentz, Polarization rotation and the third Stokes parameter: the effects of spacecraft attitude and Faraday rotation, in IEEE Transactions on Geoscience and Remote Sensing, vol. 44, no. 3, pp. 506-515, March 2006, doi: 10.1109/TGRS.2005.858413.

[2] T. Meissner and F. Wentz, Ocean Retrievals for WindSat, 2006 IEEE MicroRad, 2006, pp. 119-124, doi: 10.1109/MICRAD.2006.1677074.

[3] T. Meissner and F. Wentz, Intercalibration of AMSR-E and WindSat brightness temperature measurements over land scenes, 2010 IEEE International Geoscience and Remote Sensing Symposium, 2010, pp. 3218-3219, doi: 10.1109/IGARSS.2010.5649513.

4] T. Meissner and F. Wentz, The Emissivity of the Ocean Surface Between 6 and 90 GHz Over a Large Range of Wind Speeds and Earth Incidence Angles, in IEEE Transactions on Geoscience and Remote Sensing, vol. 50, no. 8, pp. 3004-3026, Aug. 2012, doi: 10.1109/TGRS.2011.2179662.

[5] T. Meissner, F. Wentz and D. Draper, 2012, GMI Calibration Algorithm and Analysis Theoretical Basis Document, report number 041912, Version-G, Remote Sensing Systems, Santa Rosa, CA, 124 pp. https://doi.org/10.56236/RSS-au. 4

[6] F. Wentz and D. Draper, 2016, On-Orbit Absolute Calibration of the Global Precipitation Measurement Microwave Imager. J. Atmos. Oceanic Technol., 33, 1393–1412, DOI: 10.1175/JTECH-D-15-0212.1.

[7] F. Wentz and T. Meissner, 2016, Atmospheric absorption model for dry air and water vapor at microwave frequencies below 100?GHz derived from spaceborne radiometer observations, Radio Sci., 51, 381– 391, doi:10.1002/2015RS005858.

End of document